Neuron, Vol. 40, 859–869, November 13, 2003, Copyright ©2003 by Cell Press

Mirror-Symmetric Tonotopic Maps in Human Primary Auditory Cortex

Elia Formisano,[1] Dae-Shik Kim,[2] Francesco Di Salle,[3] Pierre-Francois van de Moortele,[2] Kamil Ugurbil,[2] and Rainer Goebel[1,*]
[1]Department of Cognitive Neuroscience
Faculty of Psychology
Universiteit Maastricht
Postbus 616
6200MD Maastricht
The Netherlands
[2]Center for Magnetic Resonance Research (CMRR)
University of Minnesota Medical School
2021 Sixth Street S.E.
Minneapolis, Minnesota 55455
[3]Department of Neuroradiology
Federico II University
Nuovo Policlinico
Via Sergio Pansini 5
80131 Naples
Italy

Summary

Understanding the functional organization of the human primary auditory cortex (PAC) is an essential step in elucidating the neural mechanisms underlying the perception of sound, including speech and music. Based on invasive research in animals, it is believed that neurons in human PAC that respond selectively with respect to the spectral content of a sound form one or more maps in which neighboring patches on the cortical surface respond to similar frequencies (tonotopic maps). The number and the cortical layout of such tonotopic maps in the human brain, however, remain unknown. Here we use silent, event-related functional magnetic resonance imaging at 7 Tesla and a cortex-based analysis of functional data to delineate with high spatial resolution the detailed topography of two tonotopic maps in two adjacent subdivisions of PAC. These maps share a low-frequency border, are mirror symmetric, and clearly resemble those of presumably homologous fields in the macaque monkey.

Introduction

In the human brain, the term primary auditory cortex (PAC) refers to a region located in the transverse temporal gyrus or gyrus of Heschl (HG). Anatomically, PAC can be distinguished from the surrounding areas because of its granular (koniocortical) cytoarchitecture and its dense myelination (Hackett et al., 2001; Kaas and Hackett, 2000), features common to primary sensory areas in general. The exact number of subdivisions that form PAC remains unclear. Depending on histological criteria, what appears to correspond to the same auditory sensory cortex has been classified as one area (area 41, Brodmann, 1909) or further parcellated into two (areas TC and TD: von Economo and Koskinas, 1925; areas KAm and KAlt: Galaburda and Sanides, 1980) or three (areas Te1.0, Te1.1, and Te1.2: Morosan et al., 2001) subdivisions. Even less is known on the functional differences between these presumed subdivisions.

In the macaque monkey, anatomical information of the cortical architecture could be complemented with functional information obtained using invasive electrophysiological recordings. Results from these studies support the hypothesis that two (AI, R) (Merzenich and Brugge, 1973; Morel et al., 1993) or three (AI, R, and RT) (Kaas and Hackett, 2000) subdivisions form a primary auditory cortical "core," subserving a first stage of parallel processing of auditory information (Rauschecker et al., 1997). Neurons in these subdivisions respond best to tones at specific frequencies, exhibit narrow frequency response curves, and in at least two of these subdivisions (AI, R), form tonotopic maps. Analogously to retinotopic maps in the early areas of the visual cortex, these maps have a mirror symmetry. In AI, the most caudal of these fields, the tonotopic gradient from high to low frequencies is caudo-rostrally oriented. In R, located rostrally to AI, the tonotopic gradient is reversed such that AI and R share a low-frequency border that appears to coincide with the histologically defined border (Kaas and Hackett, 2000; Merzenich and Brugge, 1973; Morel et al., 1993). Similar to retinotopy in the visual system, tonotopy is not only a property of primary areas. Areas that belong to the so-called lateral "belt" and that subserve a second stage of the hierarchical sequence of auditory processing also display tonotopic organization, even though their neurons are less responsive to tones and prefer increasingly complex stimuli (Rauschecker et al., 1995, 1997).

A similar functional organization is expected in the human auditory cortex. Experimental evidence gathered in a number of functional neuroimaging investigations suggests a separation in "core" and "belt" areas (Di Salle et al., 2001; Seifritz et al., 2002; Wessinger et al., 2001) and the presence of multiple frequency-selective responses along the HG (Bilecen et al., 1998; Engelien et al., 2002; Lauter et al., 1985; Lockwood et al., 1999; Lütkenhöner and Steinsträter, 1998; Pantev et al., 1995; Romani et al., 1982; Schonwiesner et al., 2002; Talavage et al., 2000; Wessinger et al., 1997). However, all previous studies, including blood oxygenation level-dependent (BOLD) fMRI studies (Bilecen et al., 1998; Engelien et al., 2002; Schonwiesner et al., 2002; Talavage et al., 2000; Wessinger et al., 1997) at relatively high spatial resolution have so far failed to obtain detailed topographical representations of these frequency-selective responses. The failure to define spatial organization of frequency selective responses in the auditory cortex contrasts with the successes of fMRI in other sensory domains. In the visual domain, for example, fMRI studies have succeeded in defining the retinotopic layout and borders of early human visual areas (Sereno et al., 1995). By contrast, the number and the cortical layout of human tonotopic maps remain unknown.

In the present study, we combine ultra-high field MR

*Correspondence: r.goebel@psychology.unimaas.nl

imaging at high spatial resolution and improved specificity for functional mapping (Pfeuffer et al., 2002) with a cortex-based analysis of the functional images and depict the detailed layout of the tonotopic maps in the human PAC.

Results

Subjects (n = 6) were scanned with a 7 Tesla (T) MRI scanner. Auditory stimuli were 70 dB SPL tones at 0.5 and 3 KHz (subject #1), at 0.3, 0.5, 0.8, 1, 2, and 3 KHz (subjects #2, #4, #5, and #6), and 0.3, 1, 2, and 3 KHz (subject #3) and were binaurally presented according to an event-related stimulation scheme that minimizes interference of the scanner acoustic noise (Belin et al., 1999). Using single-shot echo-planar imaging (EPI), a linear surface coil, and an outer-volume suppression technique (Luo et al., 2001), we were able to "zoom in" on the subject's left temporal lobe and acquire high-spatial resolution ($1.2 \times 1.48 \times 2\ mm^3$) functional images of the auditory cortex. Functional images were coregistered to 3D anatomical volumes of the subject's brain collected at 1.5T (see Magnetic Resonance Imaging).

For each subject, we computed a statistical map of the response of the auditory cortex to all the tones (see Data Analysis). The activation was mainly confined to the Heschl's region, in a location that is in general agreement with what has been previously described as the location of the human primary auditory core (Brechmann et al., 2002; Di Salle et al., 2001; Engelien et al., 2002; Hall et al., 2002, 2003; Seifritz et al., 2002; Talavage et al., 2000; Wessinger et al., 2001). Because of the high spatial resolution and the suppression of the large vessel artifacts of 7T-fMRI, we found in the region delimitated caudo-medially by the Heschl's sulcus (HS) and rostro-laterally by the first transverse sulcus (FTS) the auditory activation to precisely follow the gray matter (Figure 1). Furthermore, its spatial layout showed a striking similarity to the layout of two cytoarchitectonically defined subdivisions of PAC (Te1.0 and Te1.1), as reported in recent anatomical studies (Morosan et al., 2001; Rademacher et al., 2001). Additional clusters with significant activation could be also observed outside this cortical core, especially in the adjacent caudal and lateral cortex (see Figures 1–5).

To investigate the cortical topography of frequency-selective BOLD-fMRI responses, we calculated best-frequency maps (see Data Analysis). In these maps, the color encodes the frequency of the tone that evoked the highest BOLD response (best-frequency). Maps were visualized on an inflated and a flattened representation of the subject's cortex (Figures 2–5).

Figure 2 shows a cortical surface best-frequency map obtained by comparing the responses to tones at 0.5 and 3 KHz (subject #1). Clusters with highly selective BOLD responses to lower and higher frequency tones were observed in the Heschl's region. In this subject, probably because of the presence of a duplicated HG, the most caudal aspect of the activation extended beyond the first (anterior) HG and occupied partially the second (posterior) HG. The spatial arrangement of the selective responses on the cortical surface suggested the existence of two mirror-symmetric representations of the sound frequencies along a caudomedial-rostrolateral direction. Assuming a smooth, continuous representation of the frequencies between 0.5 and 3 KHz, in the caudal region, the frequency selectivity gradient from high to low would be caudomedial-rostrolaterally oriented; in the rostral region, the representation of the frequencies has a reverse order. The two maps' relative anatomical location and the orientation of their tonotopic gradient suggest that these two regions might be the human homologs of monkey areas AI and R (hAI and hR) (Kaas and Hackett, 2000; Merzenich et al., 1973; Morel et al., 1993).

Figure 3A shows a best-frequency map obtained on the basis of the responses to six frequencies: 0.3, 0.5, 0.8, 1, 2, and 3 KHz (subject #2). In this case, the cortical topography of the tonotopic maps could be investigated in more detail, and the spatial arrangement of best-frequency clearly indicated the presence of two mirror-symmetric tonotopic maps. In a caudal region of the HG, proceeding from caudal to rostral locations, BOLD responses showed progressively reduced amplitude for high frequencies and increased amplitude for low frequencies. In a rostral region, BOLD responses exhibited an opposite pattern (Figure 3A). Additional clusters showing frequency-selective BOLD responses, but a less clear and less replicable topographical arrangement, could be observed lateral to these two regions (see also Figures 4 and 5). These clusters might belong to the so-called belt of auditory areas, in which responses to tones are weaker and less specific than in the primary areas (Rauschecker et al., 1995, 1997; Tian et al., 2001). Figures 3B and 3C illustrate a further analysis that we performed to investigate the frequency selectivity of auditory BOLD responses. Figure 3B shows the average best-frequency in a set of cortical clusters located in the two regions (a–f in Figure 3A). It can be seen that, moving along a line defined by connecting the spatial locations of clusters with highest selectivity, best-frequency monotonically decreases between "a" and "c" and monotonically increases between "c" and "f," suggesting that the border between the two presumed tonotopic subdivisions is located approximately around "c." Figure 3C displays frequency tuning curves of highly selective voxels from the same set of cortical clusters. Frequency tuning curves were obtained by calculating the amplitude of BOLD responses to tones at different frequencies (see Data Analysis) and indicate that the amplitude of BOLD responses monotonically decreases with increasing difference between stimulation frequency and best-frequency and further highlight the reversal of the tonotopic gradient around "c."

To determine objectively whether the observed topographical arrangement of best-frequency reflects the existence of mirror-symmetric tonotopic maps, we adapted to our auditory data a field sign mapping method, as has been proposed for the analysis of retinotopic visual areas (Sereno et al., 1995) (see Data Analysis). Figure 4 shows the tonotopic-field sign maps we obtained in subject #2 (Figures 4A–4C) and subject #3 (Figure 4D). Blue color in the caudal area (hAI) indicates that the direction of the local low-to-high tonotopic gradient follows the direction indicated by the arrow (see insert in Figure 4A). Conversely, green color in the rostral area (hR) indicates a mirror representation of the low-

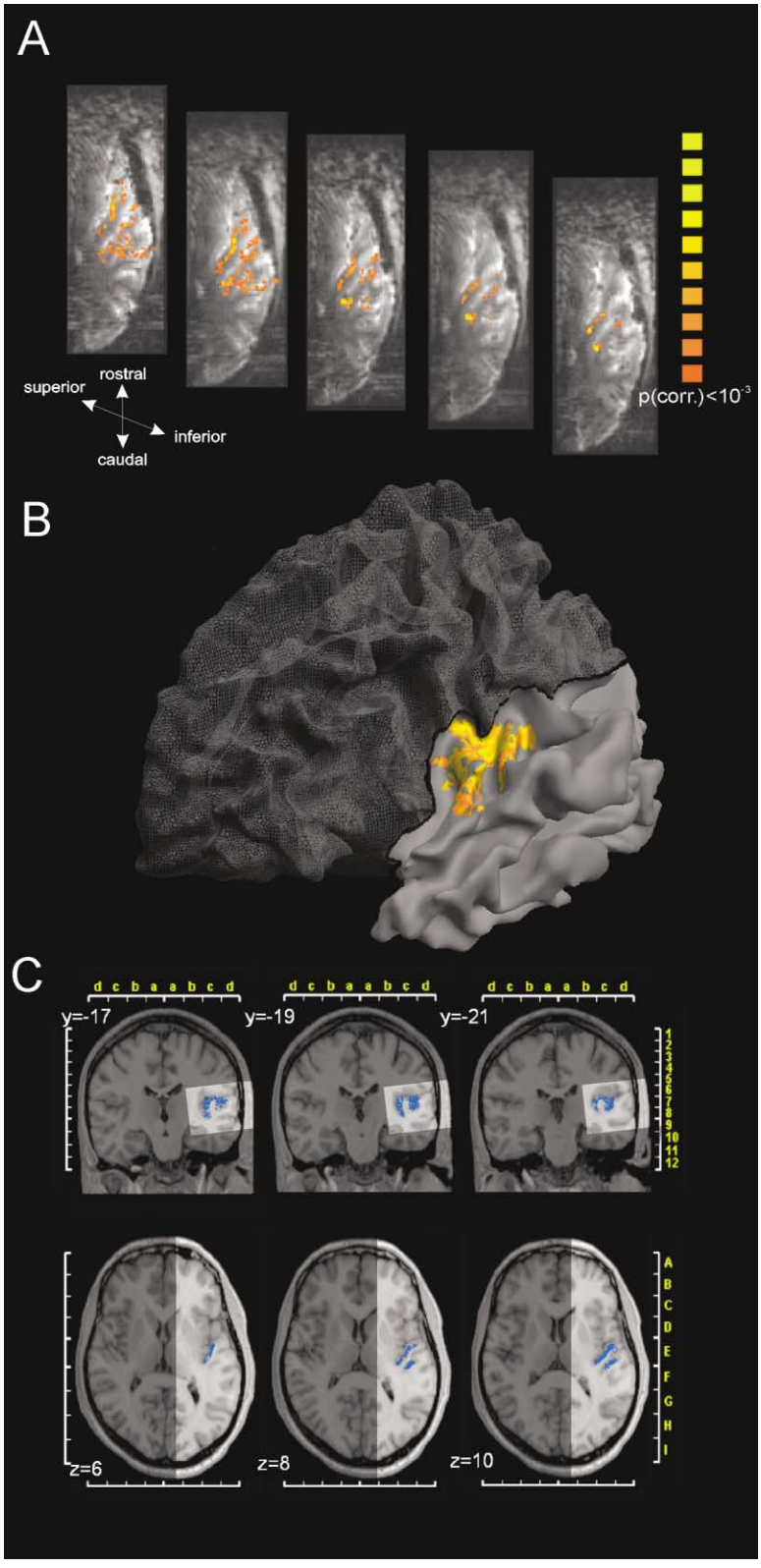

Figure 1. Localization of the Primary Auditory Cortex at 7 Tesla

A statistical map of the overall auditory cortex response to six frequencies (subject #2, frequency range 0.3–3 KHz) is superimposed on selected transverse echo-planar-imaging slices collected at 7T (A), on a mesh reconstruction of the subject's cortex, after part of the parietal lobe has been virtually removed for a better visualization of the activation in the Heschl's gyrus (B) and on coronal ($y = -17$, $y = -19$, $y = -21$) and transverse ($z = 6$, $z = 8$, $z = 10$) anatomical slices in standard Talairach space (C). In (C), lighter gray indicates the region of temporal lobe that was covered by the functional slices.

to-high local tonotopic gradient. These results confirmed our previous observations, showed a high reproducibility both for intrasubject (Figures 4B and 4C) and intersubject (Figures 4A and 4D, see also Figure 5) comparisons, and allowed us to outline the low-frequency border shared by the two areas (see dotted lines in Figure 4) in correspondence of the reversal of the field sign (Sereno et al., 1995).

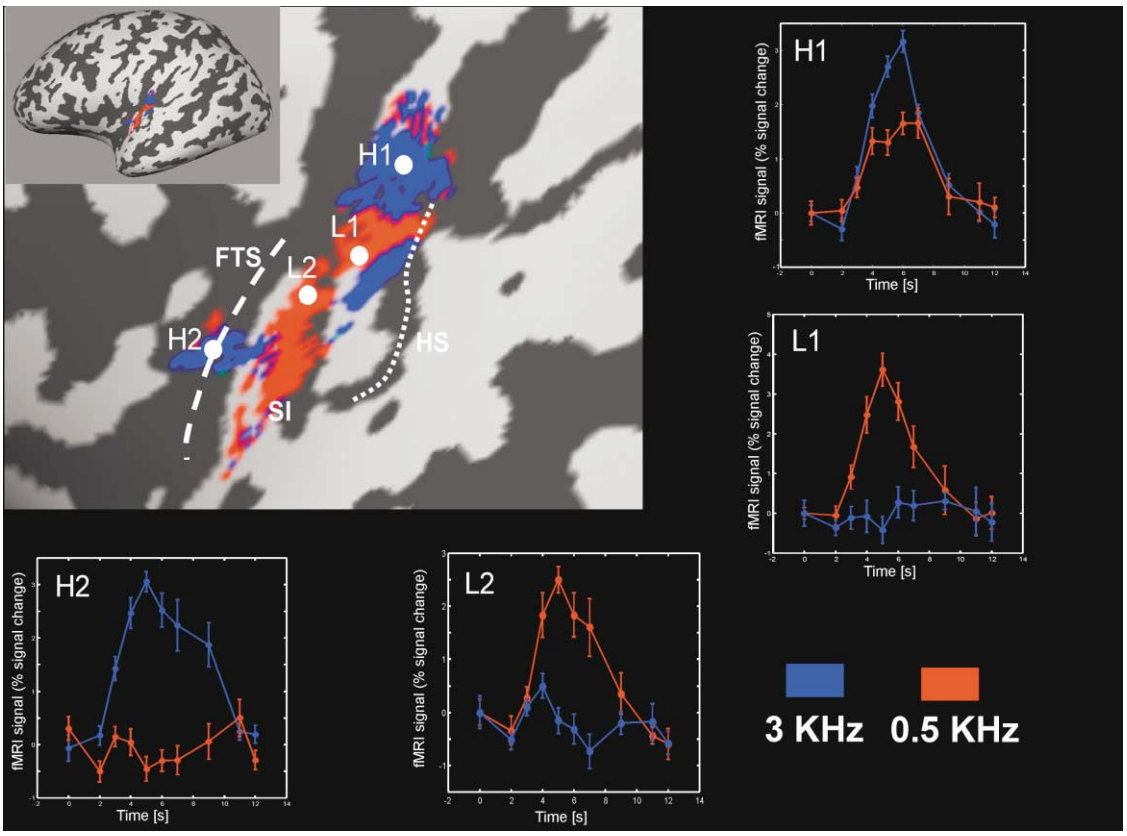

Figure 2. Spatial Layout and Average Time Courses of Frequency-Selective Responses in the Primary Auditory Cortex

A best-frequency map (subject #1; statistical analysis based on two frequencies [3 KHz, blue; 0.5 KHz, red]) is displayed on an inflated representation of the subject's cortex. In a caudal region of the activated auditory cortex, cortical clusters responding preferably to 3 KHz tones are located caudo-medially (H1), and cortical clusters responding preferably to 0.5 KHz tones are located rostro-laterally (L1). In a rostral region, cortical clusters responding preferably to 3 KHz tones are located rostro-laterally (H2), and cortical clusters responding preferably to 0.5 KHz tones caudo-medially (L2). Error bars indicate standard error of the mean. Note that this spatial arrangement of frequency-selective responses is compatible with the existence of two mirror-symmetric tonotopic maps with a rostro-caudal axis. FTS = first transverse sulcus; HS = Heschl's sulcus; SI = sulcus intermedius.

Figures 5 illustrates the cortical best-frequency maps and corresponding PAC subdivisions (in standard anatomical projections, Talairach and Tournoux, 1988) in subjects #4, #5, and #6. Maps and PAC subdivisions were obtained using identical methods and an identical set of six frequencies as in subject #2 (Figure 3) and provide a further confirmation of the reproducibility of our results. It can be noticed that, although the activation often occupies a larger expanse of cortex, two mirror-symmetric gradients (high-to-low, low-to-high) of best-frequencies can be consistently observed moving from the caudomedial extremities of the HS to rostrolateral locations along the first transverse sulcus FTS.

Discussion

Our ultra-high magnetic field imaging study provides new, compelling evidence for functional subparcellation of human PAC and thus extends previous results obtained invasively in monkeys to the human brain. Two mirror-symmetric representations of sound frequency appear to be contained in a region that significantly responds to simple tones and that is presumably included within the cytoarchitectonically delineated primary auditory sensory cortex.

Several reasons might explain why these maps could be convincingly observed in our, but not in previous, BOLD-fMRI studies. First, the silent event-related paradigm allowed us to image the auditory cortex without the interference of the loud (~100 dB) background acoustic noise, which might have been a severe limitation in previous studies using a conventional blocked or a continuous stimulation paradigm (Bilecen et al., 1998; Schonwiesner et al., 2002; Talavage et al., 2000; Wessinger et al., 1997). Second, we examined the spatial pattern of BOLD responses to up to six different frequencies using a cortical-surface-based reference system. In previous studies (Bilecen et al., 1998; Engelien et al., 2002; Talavage et al., 2000; Wessinger et al., 1997), inferences on the cortical layout of one or multiple tonotopic maps have been based only on the analysis of the relative displacement of the foci of BOLD responses to a very small number (two or three) of frequencies or ranges of frequencies. In addition, analysis in all previous studies has been conducted only on sets of two-dimensional (2D) slices or in a three-dimensional (3D) brain volume

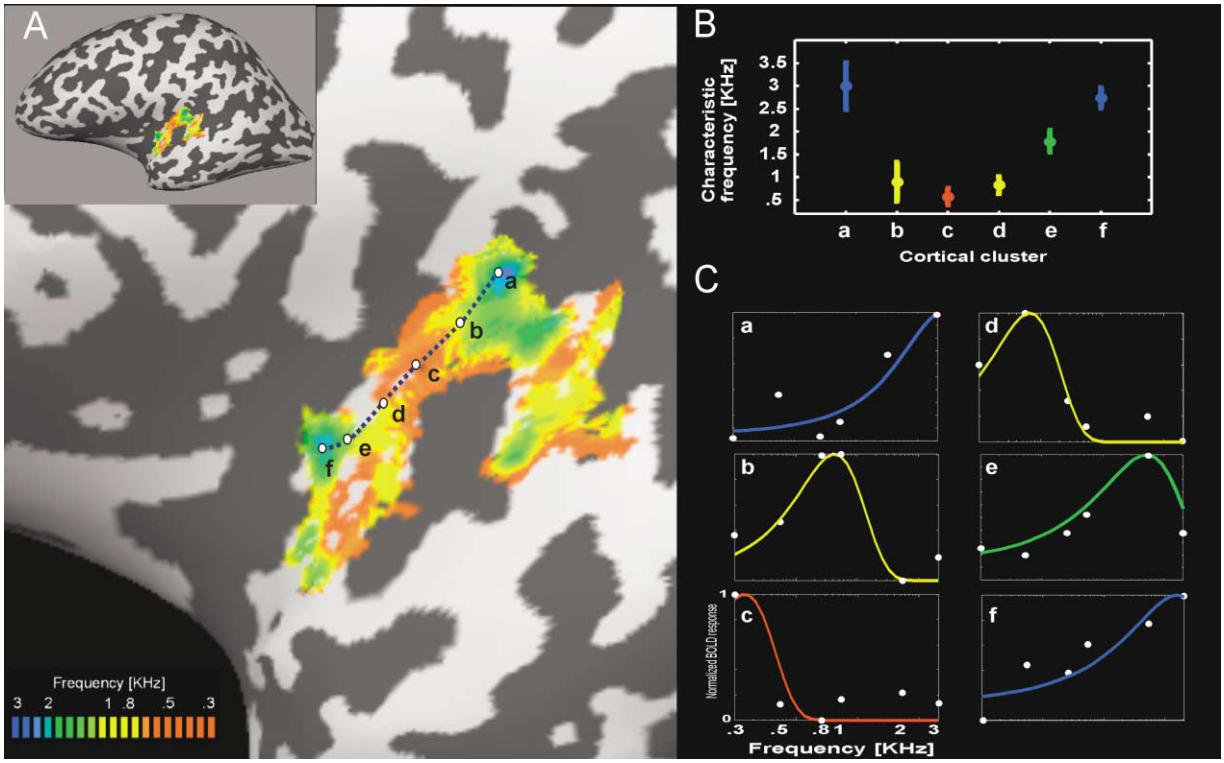

Figure 3. Spatial Layout, Best-Frequency, and Tuning Curves of Frequency-Selective Responses in Primary Auditory Cortex

(A) A best-frequency map (subject #2; statistical analysis based on six frequencies [0.3, 0.5, 0.8, 1, 2, and 3 KHz]) is displayed on an inflated representation of the subject's cortex. Color indicates the stimulus frequency that evoked the highest BOLD response. The spatial arrangement of best-frequencies reveals the existence in the human primary auditory cortex of two continuous representations of frequency (tonotopic maps) presenting a mirror symmetry along the rostral-caudal direction.

(B) Average best-frequency in a set of $\sim$5 mm^2 cortical clusters (a, b, c, d, e, and f) located in the activated PAC. Error bars indicate the standard deviation computed over best-frequencies of individual voxels indexed by these cortical clusters. In the caudomedial region (clusters a–c), the best-frequency gradient from high to low is caudo-rostrally oriented. In the most rostral region (clusters c–f) the best-frequency gradient reverses. The two tonotopic maps appear to share a common low-frequency border approximately in "c" (see also Figure 4).

(C) Frequency tuning curves for highly selective voxels from the clusters a, b, c, d, e, and f . Continuous lines show the fitting of the normalized amplitude of event-related averages of the BOLD responses to the six frequencies with a Gaussian function (see Data analysis).

and was not based on an explicit representation of the subject's cortex as in the present study. Finally, because of the lower contrast-to-noise and lower inherent image signal-to-noise, the spatial resolution utilized in the previous studies conducted with conventional low-field fMRI was significantly coarser compared to our 7 Tesla investigation. More importantly, spatial accuracy (specificity) of BOLD mapping signals achievable with conventional low-field fMRI is expected to be significantly degraded at lower magnetic field relative to 7T (Ugurbil et al., 2003) and might have been insufficient for an adequate mapping of the small auditory areas.

Our findings are consistent with those of studies in which intracortical auditory event-related potentials (ERPs) were recorded using depth electrodes (Liegeois-Chauvel et al., 1991, 1994). In Liegeois-Chauvel et al. (1994), the PAC was partitioned into two subdivisions, labeled respectively as the "extreme dorso-posterior-medial" region (located in the extreme posterior tip of the Heschl's gyrus) and the "dorso-posterior intermediate" region (located few millimeters more anterior and more lateral to the other region). The anatomical locations of these subdivisions and their relative displacement closely resemble those of our noninvasively mapped caudal and rostral subdivisions of PAC. The orderly frequency progression in the HG reported in another study using implanted microelectrodes in surgical patients (Howard et al., 1996) is also compatible with the tonotopic gradient in our caudal subdivision.

Electroencephalography (EEG) and magnetoencephalography (MEG) also contributed to the investigation of tonotopy of the human auditory cortex (Huotilanen et al., 1995; Lütkenhöner and Steinsträter, 1998; Lütkenhöner et al., 2003a; Pantev et al., 1995, 1996; Romani et al., 1982; Scherg et al., 1989; Yamamoto et al., 1992). Typically, in these studies, the tonotopic layout of an auditory cortical field is inferred by relating changes in sound frequency to shifts of orientation or spatial locations of dipoles, which are assumed to generate the scalp distribution of the evoked potential or magnetic field in specified time windows. Several difficulties arise when trying to link these frequency-dependent dipole shifts with the pattern of hemodynamic activation observed in our fMRI study. First, fMRI and EEG/MEG are based on very different biophysical mechanisms and may reflect different aspects of neuronal activity (Dale and Halgren, 2001). Second, because the neural activities of at least two closely located fields of the PAC are

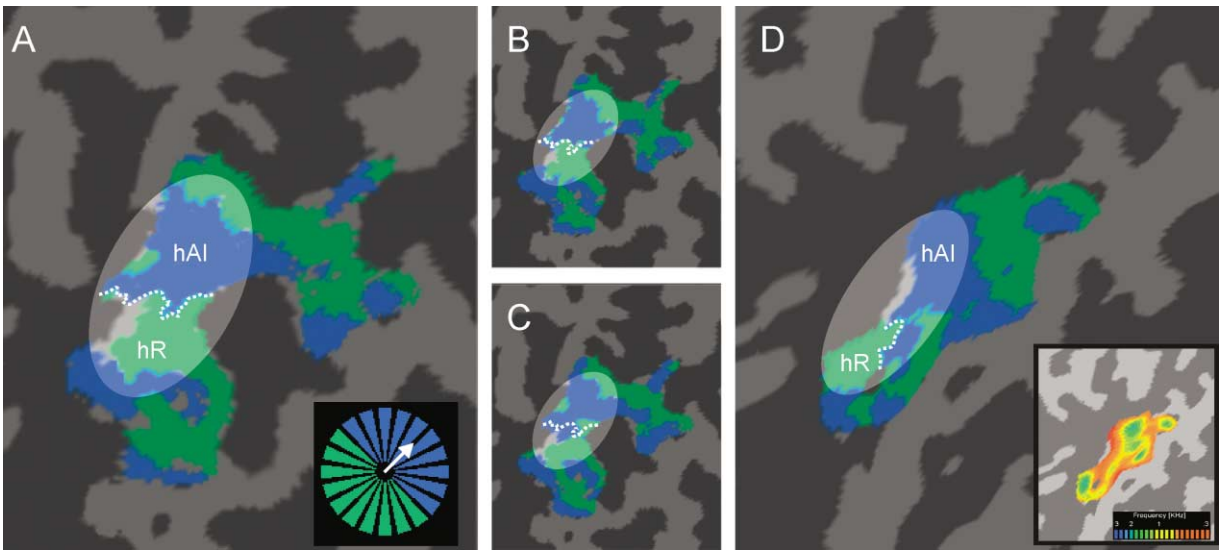

Figure 4. Tonotopic Field Sign Maps of the Human Primary Auditory Cortex

Blue and green colors indicate maps with mirror-symmetric representation of the low-to-high tonotopic gradient (see Data Analysis for details). The reversal of the field sign defines the low-frequency border between area hAI and area hR (see dotted line). In (A)–(C) tonotopic field sign maps of subject #2 were obtained from the best-frequency map shown in Figure 3 (A) and from best-frequency maps computed using only the first (B) or the second (C) half of collected data, respectively. The insert in (D) shows the best-frequency map used to compute the field sign map of subject #3.

likely to present a consistent temporal overlap (Liegeois-Chauvel et al., 1994), their modeling with equivalent dipoles may be problematic (scalp-recorded fields produced by multiple, closely located, simultaneously active current sources and those produced by a single dipole cannot be easily distinguished). Third, because tonotopic cortex in the different auditory subdivisions is variously oriented, the observed shift of dipole locations may result from a complexly weighted contribution of their activity rather than being univocally related to the activity of a single subdivision (Eggermont and Ponton, 2002). Finally, many of the EEG/MEG studies on tonotopy have focused on a component, the N100(m), which is likely to represent activity of secondary auditory areas (planum temporale) and whose frequency dependence is still controversial (for a recent discussion of the conflicting results on the tonotopy of the N100, see Lütkenhöner et al., 2003a).

Notwithstanding these cautionary remarks, it is interesting to note that the dipole-based source localization of the scalp-recorded auditory evoked potential and magnetic field recorded about 19–30 ms after stimulus onset (Scherg et al., 1989; Schneider et al., 2002; Pantev et al., 1995; Yvert et al., 2001) is compatible with our fMRI-based localization of the PAC. Opposite frequency-dependent shifts of the equivalent dipole location, however, have been reported which are either compatible with the tonotopic gradient of hAI (N19m-P30m response in Scherg et al., 1989) or with the tonotopic gradient of hR (Pam response in Pantev et al., 1995). This might be explained by methodological differences but also by assuming that (1) in the human PAC two closely located primary cortical fields are present, (2) their tonotopic gradient is oriented in opposite directions, and (3) their activity overlaps in time. The first two points are supported by our data; the third is supported by intracortical recordings (Liegeois-Chauvel et al., 1994) and by recent analyses of transient (Lütkenhöner et al., 2003b) and steady-state MEG responses (Gutschalk et al., 1999). Future studies combining high spatial resolution fMRI and EEG-MEG in the same subjects may help in relating results on tonotopy obtained using a single neuroimaging technique.

The tonotopic maps of the human PAC as revealed by our BOLD fMRI measurements are remarkably similar to the tonotopic maps as described in invasive electrophysiological studies in the macaque monkey (Kaas and Hackett, 2000; Merzenich and Brugge, 1973; Morel et al., 1993). Maps of neural best-frequencies in these as well as in studies in other animal species are typically obtained at low sound levels, 0–20 dB above the response threshold. In contrast, our maps were obtained at a sound level of 70 dB SPL. Whereas this intensity level is lower than levels used in previous fMRI investigations of tonotopy, it is still considerably higher than the intensity of stimuli typically used in electrophysiological recordings in animals.

It is known that frequency selectivity decreases with increasing sound level, suggesting that weaker stimuli are better suited to reveal tonotopy. However, fMRI, in comparison to single-cell recording, is less sensitive to weak and spatially restricted activity. Stronger stimuli are, thus, required to elicit measurable responses. On the other hand fMRI provides extended (though discrete) coverage of large volumes. Therefore data describing an extended region can be statistically integrated across space to reveal tonotopic organization. The optimal sound level for mapping tonotopy with fMRI is, thus, expected to be higher than for single-cell recording.

It should be noted, however, that several investiga-

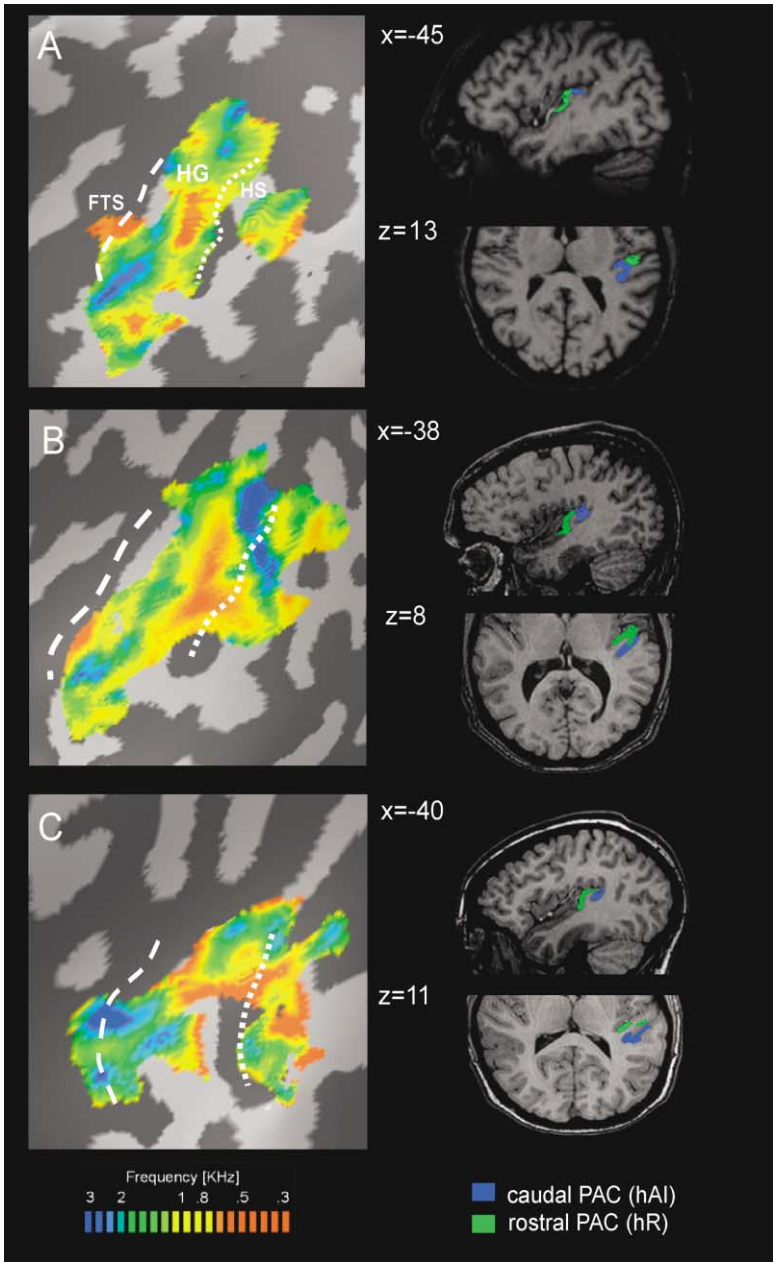

Figure 5. Best-Frequency Maps and Corresponding PAC Subdivisions in Subjects #4, #5, and #6

([A–C], left column) Cortical best-frequency maps are displayed on an inflated representation of the subjects' cortex (subject #4 [A], subject #5 [B], subject #6 [C]). Statistical analysis is based on six frequencies (0.3, 0.5, 0.8, 1, 2, and 3 KHz), and color indicates the stimulus frequency that evoked the highest BOLD response. ([A–C], right column) PAC subdivisions, as defined by the mirror-symmetric tonotopic maps, are visualized on selected sagittal and transverse anatomical slices in standard Talairach space. FTS = first transverse sulcus; HG = Heschl's gyrus; HS = Heschl's sulcus.

tions in anesthetized animals have shown that stimuli at high intensity levels evoke reduced response rates in a percentage of neurons in the primary auditory cortical field (cat: Schreiner et al., 1992; Heil et al., 1994; Phillips et al., 1994; ferret: Kowalski et al. 1995). Furthermore, in the anesthetized cat, a tonotopic layout is observed with near-threshold stimuli but may be absent or altered at high intensity levels (Phillips et al., 1994).

Our findings demonstrate for awake humans that responses are still selective to frequency and that tonotopic maps exist in human PAC at 70 dB SPL. These findings are compatible with the results of a recent investigation of frequency and intensity response properties of single neurons in the auditory cortex of the behaving macaque monkey (Recanzone et al., 2000). Frequency response areas of AI neurons reported in this study indicate for intensity levels around 70 dB SPL that neurons respond to a relatively broad range of frequencies. However, their response is still highest at frequencies close to the frequency that produces a driven response at the lowest intensity (Recanzone et al., 2000). Our approach of computing the best-frequency maps based on the frequency evoking the highest BOLD response is robust to a partial loss of frequency selectivity and to a certain degree of overlap of responses, which is expected at the intensity level of our stimulus. Further investigations employing a broader combination of intensities and frequencies in human experiments will help test this possibility.

More generally, it should be noted that BOLD fMRI measurements reflect the hemodynamic changes related to the spiking and subtreshold activity of large

ensembles of neurons (Logothetis et al., 2001) and that, even at the relatively high spatial resolution achievable at ultra-high magnetic field, the spatial scale of the investigation is much coarser than in invasive electrophysiological recordings. Caution should thus be taken in judging similarities and dissimilarities between fMRI results and results from electrophysiological investigations typically based on spike counts of single units.

Importantly, our results are consistent with recent studies of the auditory cortex in anesthetized animals that employed optical imaging, a technique based on physiological principles closely related to BOLD fMRI (Harel et al., 2000; Versnel et al., 2002). In Harel et al. (2000), tonotopic maps of the auditory fields of the chinchilla that resembled those derived electrophysiologically (Harrison et al., 1996) were obtained using stimuli identical to ours and sound levels up to 80 dB SPL. In Versnel et al. (2002) optical tonotopic maps of the ferret's auditory cortex were shown to be largely independent of the (supratreshold) sound level and also of the type of narrowband stimulus used (pulsed, amplitude-, or frequency-modulated) and the modulation rate. Compared to these maps, the tonotopic layout of our human tonotopic maps appears to show a greater intersubject variability. This is possibly a consequence of the greater anatomical variability of the human auditory cortex but also of the fact that our subjects were awake and that response properties of neurons are more variable or subject to modulation in the awake state than in the anesthetized state. Future studies employing a wide range of techniques in the same animal will be particularly relevant in elucidating the relation between electrophysiologically derived and hemodynamic/metabolic tonotopic maps and their dependence on the state of the animal.

Our findings have a great practical relevance for future studies of human audition. The identification of primary auditory subdivisions represents an essential step in understanding the cortical organization of the human brain underlying the perception of sound, including speech and music. Because of the great interindividual anatomical variability of the Heschl's region (Penhune et al., 1996) and because of the weak correspondence between commonly used anatomical landmarks and architectonically defined subdivisions (Morosan et al., 2001), this identification can only be obtained with functional mapping in individual brains. In few pathological cases this might be carried out invasively using intrasurgical event-related potential recordings (Liegeois-Chauvel et al., 1991, 1994). Our results demonstrate that with silent event-related fMRI at high spatial resolution and tonotopic mapping, such information can be unambiguously obtained in normal volunteers.

The specific neurocomputational role of these two representations of sound frequency within PAC cannot be explained exclusively on the basis of available data. Various invasive methods demonstrated the existence of tonotopic maps of PAC in a number of species (Harel et al., 2000; Kaas and Hackett, 2000; Merzenich and Brugge, 1973; Merzenich et al., 1973; Morel et al., 1993; Recanzone et al., 1999) and their functional role in extracting spectral features of a sound (Read et al., 2002; Scheich, 1991). In humans, as in primates (Kaas and Hackett, 2000), it is likely that the two frequency maps subserve a first stage of parallel processing of auditory information and initiate downstream processing in the auditory "what" (rostral) and "where" (caudal) parallel functional streams (Rauschecker and Tian, 2000; Romanski et al., 1999).

We expect that tonotopic mapping in combination with a large variety of auditory stimuli will help clarify the exact contribution of these two subdivisions to auditory processing and, more generally, how topographically encoded information on sound frequency is combined with different and variously encoded information on other features of the auditory stimuli, such as duration, amplitude, bandwidth, and modulation (Brechmann et al., 2002; Di Salle et al., 2001; Hall et al., 2002; Seifritz et al., 2002; Wessinger et al., 2001) and with mechanisms of sound localization (Alain et al., 2001; Warren et al., 2002).

Experimental Procedures

Subjects

Six adult subjects (four male, two female, ages 23–38) gave their informed consent and participated in the study. Subjects were all right handed and had normal audition.

Magnetic Resonance Imaging

Functional imaging was performed at the Center for Magnetic Resonance Research (Minneapolis, MN) in a 90 cm bore 7 Tesla magnet (Magnex Scientific, Abingdon, UK) operated with a Varian (Palo Alto, CA) console. A linear surface coil (12 cm diameter) and a single-shot Gradient Recalled Blipped Echo Planar Imaging (EPI) sequence (echo time (TE) = 27 ms, flip angle (FA) = 90°, TR = 20 s) were used for collecting high-resolution functional images of the left temporal lobe. Localized adjustments of the first order shims, and when needed of the second order shims, were performed in the temporal cortex with FAST(EST)MAP (Gruetter and Tkac, 2000). In order to acquire single-shot high-resolution EPI images, an outer-volume suppression technique with adiabatic pulses (see Luo et al., 2001; Pfeuffer et al., 2002, for details) was used, yielding a reduced field-of-view of 15.36 cm (antero-posterior) × 6.50 cm (left-right) and a nominal resolution of 1.20 × 1.48 × 2.00 mm^3.

Within each 7T functional session, T1-weighted EPI images (obtained with an inversion preparation module, inversion time TI = 1.5 s, FA = 90°, TE = 27 ms) were also collected at the same slice locations. These images were used to coregister 7T data sets with a whole-head 3D anatomical dataset obtained from the same subjects using a conventional 1.5T clinical scanner (MAGNETOM Vision; Siemens, Erlangen, Germany) and a three-dimensional T1-fast-low-angle shot (FLASH) sequence (180 slices, TR = 30 ms; TE = 5 ms; FA = 40°; FOV = 256 × 256 mm^2; matrix = 256 × 256; voxel size = 1 × 1 × 1 mm^3). After coregistration, the 1.5T 3D data set was used for visualization of the functional 7T data (see Data Analysis).

fMRI and Stimulation Paradigm

Auditory stimuli consisted of binaural 3 s sine tones with the carrier frequency at 0.3, 0.5, 0.8, 1, 2, or 3 KHz, pulsed with a 8 Hz square wave (rise/fall time = 5 ms, plateau = 30 ms, interstimulus interval [ISI] = 50 ms). Stimuli were generated and delivered using a system that included a personal computer, custom-made software, a commercial sound card, and a commercial MR-compatible stimulation device (Commander XG, Resonance Technology Inc.), which uses an air-conducting tube in combination with a nonmagnetic piezoelectric transducer. Before the measuring sessions, the stimulation system was calibrated by means of a condenser microphone (Larson Davis, 2540), a precision sound level meter (Bruel & Kjaer, 2231), and a calibrator (Larson Davis, CA250). The system does not induce artifacts in MR images, has a flat frequency response, and accurately preserves tone frequencies in the range of the stimulation frequencies used (0.3–3 KHz). The intensity of the output stimulus was set to 70 dB SPL for all subjects and for all the frequencies. Special

padded headphones provided an overall attenuation of ~30 dB to the environmental noise.

Functional images were collected using a stroboscopic event-related scheme that has been shown to avoid any interference of the scanner acoustic noise (Belin et al., 1999). During a scanning session several functional runs were collected. In each separate run, a tone at one of the six frequencies was used for stimulation. Subjects underwent two (with tones at 0.5 and 3 KHz, subject #1), six (with tones at 3, 0.3, 1, 2, 0.8, and 0.5 KHz, subjects #2, #4, #5, and #6) or four (with tones at 0.3, 3, 2, and 1 KHz, subject #3) functional runs. A functional run included 48 multislices (20 slices, matrix size = 128×44, total acquisition time = 1.35 s) EPI measurements. Each EPI measurement was collected at regular 20s intervals with an auditory stimulus being presented at variable offsets (0, 2, 3, 4, 5, 6, 7, and 9 s) before each scan. This acquisition scheme allowed the reconstruction of the entire time course of six stimulus-evoked BOLD responses for each run/frequency.

Data Analysis

Functional and anatomical images were analyzed using Brain Voyager 2000 (Brain Innovation, Maastricht, The Netherlands). After preprocessing (interscan slice time-correction, 3D motion correction, high-pass filtering), functional time series were interpolated to $1 \times 1 \times 1$ mm^3 and coregistered to 3D anatomical images that were used for automatic cortical surface reconstruction, inflation, and flattening and for the generation of cortical masks that were used as a constraint for the analysis of functional time series (Kriegeskorte and Goebel, 2001; Formisano et al. 2002). Statistical maps were obtained on the basis of a single-subject analysis. For each subject, a general linear model (GLM) that included a linear predictor for each frequency was computed. The overall model fit was assessed using an F statistic. The obtained p values were corrected for multiple comparisons using a cortex-based Bonferroni adjustment, i.e., the number of comparisons considered was reduced by limiting the analysis to gray matter voxels (Formisano et al., 2002).

The cortical layout of tonotopic responses was investigated using best-frequency maps. For each voxel with a significant ($p < 10^{-3}$, corrected) response to tones, best-frequency was estimated as the frequency at which the averaged stimulus-related BOLD response had the highest amplitude. Maps of best-frequency were obtained by color-coding the estimated best-frequency using two colors (blue and red, see Figure 2) or a logarithmic blue-green-yellow-red color scale (see Figures 3A, 4D, and 5). These maps were projected on folded and morphed (inflated and flattened) polygon meshes (~150,000 vertices) representing the subject's cortical sheet. A continuous representation of best-frequency was obtained by cortical smoothing of the projected map using a 2-neighbor vertices spatial filter.

In subject #2, for each voxel indexed by the cortical maps, frequency tuning curves were computed by fitting the normalized BOLD responses with a Gaussian function. Post hoc estimates of best-frequency and selectivity were obtained, respectively, as the frequency corresponding to the maximum of the Gaussian fit and as the ratio between best-frequency and full-width at half maximum (FWHM) of the Gaussian fit.

Tonotopic field sign maps (Figure 4) were obtained from smoothed versions of a best-frequency map as follows. First, a frequency gradient map was obtained by computing locally the direction of increasing frequency at each vertex of a flattened cortical mesh. Second, a tonotopic axis was defined in correspondence with a line connecting the two high-frequency peaks in the caudo-medial and rostro-lateral portions of activated PAC (see white arrow in the insert in Figure 4A). Finally, gradient directions obtained at each vertex were colored using a binary code: a vertex was color-coded in blue if the associated local direction was included within a $\pm 90°$ interval centered around the tonotopic axis (see color wheel in the insert in Figure 4A); conversely, a vertex was color-coded in green if the associated local direction corresponded to a mirror representation of the same interval. Note that, whereas two stimulus parameters (polar angle and eccentricity) can be used for an objective definition of a field sign in the retinotopic mapping of the visual cortex (Sereno et al., 1995), in our tonotopic mapping only one stimulus parameter is available (stimulus frequency). In our method the definition of a tonotopic axis is thus required in order to reduce the sign-mapping problem to one dimension. Our choice for this axis is appropriate for the auditory fields that are activated with high reproducibility in our subjects (see highlighted region in Figure 4). Tonotopic mapping of fields outside this region requires the choice of a different axis.

Acknowledgments

Work performed at the University of Minnesota was supported by NIH grants RR08079, EB00331, the Keck Foundation, and the MIND Institute. The authors are grateful to Gregor Adriany for building the surface coil, Frederic Humbert for helping with 7 Tesla measurements, Noam Harel for insightful discussions, and Nikolaus Kriegeskorte and the reviewers for useful comments on the manuscript.

Received: March 31, 2003
Revised: September 3, 2003
Accepted: September 25, 2003
Published: November 12, 2003

References

Alain, C., Arnott, S.R., Hevenor, S., Graham, S., and Grady, C.L. (2001). "What" and "where" in the human auditory system. Proc. Natl. Acad. Sci. USA *98*, 12301–12306.

Belin, P., Zatorre, R.J., Hoge, R., Evans, A.C., and Pike, B. (1999). Event-related fMRI of the auditory cortex. Neuroimage *10*, 417–429.

Bilecen, D., Scheffler, K., Schmid, N., Tschopp, K., and Seelig, J. (1998). Tonotopic organization of the human auditory cortex as detected by BOLD-FMRI. Hear. Res. *126*, 19–27.

Brechmann, A., Baumgart, F., and Scheich, H. (2002). Sound-level-dependent representation of frequency modulations in human auditory cortex: a low-noise fMRI study. J. Neurophysiol. *87*, 423–433.

Brodmann, K. (1909). Vergleichende Localisationslehre der Grosshirnrinde in ihren Prinzipien dargestellt auf Grund des Zellenhaues (Liepzig: Verlag von Johann Ambrosius Barth).

Dale, A.M., and Halgren, E. (2001). Spatiotemporal mapping of brain activity by integration of multiple imaging modalities. Curr. Opin. Neurobiol. *11*, 202–208.

Di Salle, F., Formisano, E., Seifritz, E., Linden, D.E., Scheffler, K., Saulino, C., Tedeschi, G., Zanella, F.E., Pepino, A., Goebel, R., and Marciano, E. (2001). Functional fields in human auditory cortex revealed by time-resolved fMRI without interference of EPI noise. Neuroimage *13*, 328–338.

Eggermont, J.J., and Ponton, C.W. (2002). The neurophysiology of auditory perception: from single units to evoked potentials. Audiol. Neurootol. *7*, 71–99.

Engelien, A., Yang, Y., Engelien, W., Zonana, J., Stern, E., and Silbersweig, D. (2002). Physiological mapping of human auditory cortices with a silent event-related fMRI technique. Neuroimage *16*, 944–953.

Formisano, E., Linden, D.E., Di Salle, F., Trojano, L., Esposito, F., Sack, A.T., Grossi, D., Zanella, F.E., and Goebel, R. (2002). Tracking the mind's image in the brain I: time-resolved fMRI during visuospatial mental imagery. Neuron *35*, 185–194.

Galaburda, A., and Sanides, F. (1980). Cytoarchitectonic organization of the human auditory cortex. J. Comp. Neurol. *190*, 597–610.

Gruetter, R., and Tkac, I. (2000). Field mapping without reference scan using asymmetric echo-planar techniques. Magn. Reson. Med. *43*, 319–323.

Gutschalk, A., Ryuzo, M., Roth, R., Ille, N., Rupp, A., Hähnel, S., Picton, T.W., and Scherg, M. (1999). Deconvolution of 40 Hz steady-state fields reveals two overlapping source activities of the human auditory cortex. Clin. Neurophysiol. *110*, 856–868.

Hackett, T.A., Preuss, T.M., and Kaas, J.H. (2001). Architectonic identification of the core region in auditory cortex of macaques, chimpanzees, and humans. J. Comp. Neurol. *441*, 197–222.

Hall, D.A., Johnsrude, I.S., Haggard, M.P., Palmer, A.R., Akeroyd, M.A., and Summerfield, A.Q. (2002). Spectral and temporal processing in human auditory cortex. Cereb. Cortex *12*, 140–149.

Hall, D.A., Hart, H.C., and Johnsrude, I.S. (2003). Relationships between human auditory cortical structure and function. Audiol. Neurootol. *8*, 1–18.

Harel, N., Mori, N., Sawada, S., Mount, R.J., and Harrison, R.V. (2000). Three distinct auditory areas of cortex (AI, AII, and AAF) defined by optical imaging of intrinsic signals. Neuroimage *11*, 302–312.

Harrison, R.V., Kakigi, A., Hirakawa, H., Harel, N., and Mount, R.J. (1996). Tonotopic mapping in auditory areas of the chinchilla. Hear. Res. *100*, 157–163.

Heil, P., Rajan, R., and Irvine, D.R. (1994). Topographic representation of tone intensity along the isofrequency axis of cat primary auditory cortex. Hear. Res. *76*, 188–202.

Howard, M.A., Volkov, I.O., Abbas, P.J., Damasio, H., Ollendieck, M.C., and Granner, M.A. (1996). A chronic microelectrode investigation of the tonotopic organization of human auditory cortex. Brain Res. *724*, 260–264.

Huotilanen, M., Tiitinen, H., Lavikainen, J., Ilmoniemi, R.J., Pekkonen, E., Sinkkonen, J., Laine, P., and Naatanen, R. (1995). Sustained fields of tones and glides reflect tonotopy of the auditory cortex. Neuroreport *6*, 841–844.

Kaas, J.H., and Hackett, T.A. (2000). Subdivisions of auditory cortex and processing streams in primates. Proc. Natl. Acad. Sci. USA *97*, 11793–11799.

Kriegeskorte, N., and Goebel, R. (2001). An efficient algorithm for topologically correct segmentation of the cortical sheet in anatomical MR volumes. Neuroimage *14*, 329–346.

Kowalski, N., Versnel, H., and Shamma, S.A. (1995). Comparison of responses in the anterior and primary auditory fields of the ferret cortex. J. Neurophysiol. *73*, 1513–1523.

Lauter, J.L., Herscovitch, P., Formby, C., and Raichle, M.E. (1985). Tonotopic organization in human auditory cortex revealed by positron emission tomography. Hear. Res. *20*, 199–205.

Liegeois-Chauvel, C., Musolino, A., and Chauvel, P. (1991). Localization of the primary auditory area in man. Brain *114 (Part 1A)*, 139–151.

Liegeois-Chauvel, C., Musolino, A., Badier, J.M., Marquis, P., and Chauvel, P. (1994). Evoked potentials recorded from the auditory cortex in man: evaluation and topography of the middle latency components. Electroencephalogr. Clin. Neurophysiol. *92*, 204–214.

Lockwood, A.H., Salvi, R.J., Coad, M.L., Arnold, S.A., Wack, D.S., Murphy, B.W., and Burkard, R.F. (1999). The functional anatomy of the normal human auditory system: responses to 0.5 and 4.0 kHz tones at varied intensities. Cereb. Cortex *9*, 65–76.

Logothetis, N.K., Pauls, J., Augath, M., Trinath, T., and Oeltermann, A. (2001). Neurophysiological investigation of the basis of the fMRI signal. Nature *412*, 150–157.

Luo, Y., de Graaf, R.A., DelaBarre, L., Tannus, A., and Garwood, M. (2001). BISTRO: an outer-volume suppression method that tolerates RF field inhomogeneity. Magn. Reson. Med. *45*, 1095–1102.

Lütkenhöner, B., and Steinsträter, O. (1998). High-precision neuromagnetic study of the functional organization of the human auditory cortex. Audiol. Neurootol. *3*, 191–213.

Lütkenhöner, B., Krumbholz, K., and Seither-Preisler, A. (2003a). Studies of tonotopy based on wave N100 of the auditory evoked field are problematic. Neuroimage *19*, 935–949.

Lütkenhöner, B., Krumbholz, K., Lammertmann, C., Seither-Preisler, A., Steinsträter, O., and Petterson, R.D. (2003b). Localization of primary auditory cortex in humans by magnetoencephalography. Neuroimage *18*, 58–66.

Merzenich, M.M., and Brugge, J.F. (1973). Representation of the cochlear partition of the superior temporal plane of the macaque monkey. Brain Res. *50*, 275–296.

Merzenich, M.M., Knight, P.L., and Roth, G.L. (1973). Cochleotopic organization of primary auditory cortex in the cat. Brain Res. *63*, 343–346.

Morel, A., Garraghty, P.E., and Kaas, J.H. (1993). Tonotopic organization, architectonic fields, and connections of auditory cortex in macaque monkeys. J. Comp. Neurol. *335*, 437–459.

Morosan, P., Rademacher, J., Schleicher, A., Amunts, K., Schormann, T., and Zilles, K. (2001). Human primary auditory cortex: cytoarchitectonic subdivisions and mapping into a spatial reference system. Neuroimage *13*, 684–701.

Pantev, C., Bertrand, O., Eulitz, C., Verkindt, C., Hampson, S., Schuierer, G., and Elbert, T. (1995). Specific tonotopic organizations of different areas of the human auditory cortex revealed by simultaneous magnetic and electric recordings. Electroencephalogr. Clin. Neurophysiol. *94*, 26–40.

Pantev, C., Roberts, L.E., Elbert, T., Ross, B., and Wienbruch, C. (1996). Tonotopic organizazion of the sources of human auditory steady-state responses. Hear. Res. *101*, 62–74.

Penhune, V.B., Zatorre, R.J., MacDonald, J.D., and Evans, A.C. (1996). Interhemispheric anatomical differences in human primary auditory cortex: probabilistic mapping and volume measurement from magnetic resonance scans. Cereb. Cortex *6*, 661–672.

Pfeuffer, J., Van De Moortele, P.F., Yacoub, E., Smuel, A., Adriany, G., Andersen, P., Merkle, H., Garwood, M., Xiaoping, H., and Ugurbil, K. (2002). Zoomed functional imaging in the human brain at 7 Tesla with simultaneous high spatial and high temporal resolution. Neuroimage *17*, 272–286.

Phillips, D.P., Semple, M.N., Calford, M.B., and Kitzes, L.M. (1994). Level-dependent representation of stimulus frequency in cat primary auditory cortex. Exp. Brain Res. *102*, 210–226.

Rademacher, J., Morosan, P., Schormann, T., Schleicher, A., Werner, C., Freund, H.J., and Zilles, K. (2001). Probabilistic mapping and volume measurement of human primary auditory cortex. Neuroimage *13*, 669–683.

Rauschecker, J.P., and Tian, B. (2000). Mechanisms and streams for processing of "what" and "where" in auditory cortex. Proc. Natl. Acad. Sci. USA *97*, 11800–11806.

Rauschecker, J.P., Tian, B., and Hauser, M. (1995). Processing of complex sounds in the macaque nonprimary auditory cortex. Science *268*, 111–114.

Rauschecker, J.P., Tian, B., Pons, T., and Mishkin, M. (1997). Serial and parallel processing in rhesus monkey auditory cortex. J. Comp. Neurol. *382*, 89–103.

Read, H.L., Winer, J.A., and Schreiner, C.E. (2002). Functional architecture of auditory cortex. Curr. Opin. Neurobiol. *12*, 433–440.

Recanzone, G.H., Schreiner, C.E., Sutter, M.L., Beitel, R.E., and Merzenich, M.M. (1999). Functional organization of spectral receptive fields in the primary auditory cortex of the owl monkey. J. Comp. Neurol. *415*, 460–481.

Recanzone, G.H., Guard, D.C., and Phan, M.L. (2000). Frequency and intensity response properties of single neurons in the auditory cortex of the behaving macaque monkey. J. Neurophysiol. *83*, 2315–2331.

Romani, G.L., Williamson, S.J., and Kaufman, L. (1982). Tonotopic organization of the human auditory cortex. Science *216*, 1339–1340.

Romanski, L.M., Tian, B., Fritz, J., Mishkin, M., Goldman-Rakic, P.S., and Rauschecker, J.P. (1999). Dual streams of auditory afferents target multiple domains in the primate prefrontal cortex. Nat. Neurosci. *2*, 1131–1136.

Scheich, H. (1991). Auditory cortex: comparative aspects of maps and plasticity. Curr. Opin. Neurobiol. *1*, 236–247.

Scherg, M., Hari, R., and Hämäläinen, M. (1989). Frequency-specific sources of the auditory N19–P30–P50 response detected by a multiple source analysis of evoked magnetic fields and potentials. In Advances in Biomagnetism, S. Williamson, ed. (New York: Plenum Press), pp. 97–100.

Schneider, P., Scherg, M., Dosch, G., Specht, H.J., Gutschalk, A., and Rupp, A. (2002). Morphology of Heschl's gyrus reflects enhanced activation in the auditory cortex of musicians. Nat. Neurosci. *5*, 688–694.

Schonwiesner, M., von Cramon, D.Y., and Rubsamen, R. (2002). Is it tonotopy after all? Neuroimage *17*, 1144–1161.

Schreiner, C.E., Mendelson, J.R., and Sutter, M.L. (1992). Functional topography of cat primary auditory cortex: representation of tone intensity. Exp. Brain Res. *92*, 105–122.

Seifritz, E., Esposito, F., Franciszek, H., Mustovic, H., Neuhoff, J.G.,

Bilecen, D., Tedeschi, G., Scheffler, K., and Di Salle, F. (2002). Spatio-temporal pattern of neural processing in the human auditory cortex. Science *297*, 1706–1708.

Sereno, M.I., Dale, A.M., Reppas, J.B., Kwong, K.K., Belliveau, J.W., Brady, T.J., Rosen, B.R., and Tootell, R.B. (1995). Borders of multiple visual areas in humans revealed by functional magnetic resonance imaging. Science *268*, 889–893.

Talairach, J., and Tournoux, P. (1988). Co-Planar Stereotaxic Atlas of the Human Brain (Stuttgart: G. Thieme).

Talavage, T.M., Ledden, P.J., Benson, R.R., Rosen, B.R., and Melcher, J.R. (2000). Frequency-dependent responses exhibited by multiple regions in human auditory cortex. Hear. Res. *150*, 225–244.

Tian, B., Reser, D., Durham, A., Kustov, A., and Rauschecker, J.P. (2001). Functional specialization in rhesus monkey auditory cortex. Science *292*, 290–293.

Ugurbil, K., Toth, L., and Kim, D.S. (2003). How accurate is magnetic resonance imaging of brain function? Trends Neurosci. *26*, 108–114.

Versnel, H., Mossop, J.E., Mrsic-Flogel, T.D., Ahmed, B., and Moore, D.R. (2002). Optical imaging of intrinsic signals in ferret auditory cortex: responses to narrowband sound stimuli. J. Neurophysiol. *88*, 1545–1558.

von Economo, C., and Koskinas, G.N. (1925). Die Cytoarchitektonik der Hirnrinde des erwachsenen Menschen (Vienna, Berlin: J. Springer).

Warren, J.D., Zielinski, B.A., Green, G.G., Rauschecker, J.P., and Griffiths, T.D. (2002). Perception of sound-source motion by the human brain. Neuron *34*, 139–148.

Wessinger, C.M., Buonocore, M.H., Kussmaul, C.L., and Mangun, G.R. (1997). Tonotopy in the human auditory cortex examined with functional magnetic resonance imaging. Hum. Brain Mapp. *5*, 18–25.

Wessinger, C.M., VanMeter, J., Tian, B., Van Lare, J., Pekar, J., and Rauschecker, J.P. (2001). Hierarchical organization of the human auditory cortex revealed by functional magnetic resonance imaging. J. Cogn. Neurosci. *13*, 1–7.

Yamamoto, T., Uemara, T., and Llinas, R. (1992). Tonotopic organization of human auditory cortex revealed by multi-channel SQUID system. Acta Otolaryngol. *112*, 210–214.

Yvert, B., Crouzeix, A., Bertrand, O., Seither-Preisler, A., and Pantev, C. (2001). Multiple supratemporal sources of magnetic and electric auditory evoked middle latency components in humans. Cereb. Cortex *11*, 411–423.